ISSN (Print) 1226-1750
ISSN (Online) 2233-6656
Journal of Magnetics 24(1), 62-69 (2019) https://doi.org/10.4283/JMAG.2019.24.1.062

Effects of External Magnetic Field on non-Newtonian Two Phase Fluid in an Annulus with Peristaltic Pumping

A. Riaz[1]*, A. Zeeshan[2], S. Ahmad[2], A. Razaq[1], and M. Zubair[1]

[1]*Department of Mathematics, University of Education, Lahore, Jauharabad Campus, Jauharabad 41200, Pakistan*
[2]*Department of Mathematics and Statistics, FBAS, IIU Islamabad 44000, Pakistan*

(Received 22 May 2018, Received in final form 14 December 2018, Accepted 16 December 2018)

This paper comprises the exact solutions of Non-Newtonian multiphase fluid through peristaltic pumping characteristics in an annulus having complaint walls and applied magnetic field. The mechanics of the geometry are defined cylindrical due to its large number of utilizations in medicine and biological apparatus. The external cylinder is having sinusoidal waves travelling along its walls. The problem is simplified by some suitable and valid approximations. The authors have obtained the accurate solutions of the velocities of two phases. The effects of appertaining parameters have been displayed through graphs of velocity for v and particulate phases and the behavior of curves are manipulated accordingly. It is concluded that applied magnetic field decreases the velocity of both the fluid and the particles flow.

Keywords : peristaltic flow, MHD, multiphase flow, compliant walls, annulus

1. Introduction

The phenomenon of peristalsis occurs naturally in human organs by means of incessant periodic muscular oscillations of the ducts through pumping physiological fluid. The examples include: flow of urine from kidney to bladder, bile pace in a duct, motion of food bolus in the alimentary canal, chime movement in the gastrointestinal tract, movement of eggs in the female Fallopian tube, transportation of lymph in the lymphatic vessels, vasomotion in small blood vessels and also many glandular ducts. A variety of theoretical and experimental studies has been introduced on peristaltic transport on many fluid models through various types of geometries.

Many researchers put their efforts to analyze the significant features of Newtonian and non-Newtonian fluids [1-5]. Mostly, fluids are used in industries which exhibit non-linear behavior. So a large of number of researchers and scientists have presented the problems of peristaltic transport of non-Newtonian fluid [6-12].

The studies mentioned earlier do not realize the effect of walls flexibility. The experimental studies [13, 14] emphasize the consideration of walls characteristics of the channel in peristaltic studies. To reflex the importance of wall flexibility of the channel/tube in the natural processes that exist in the industry and physiology, the peristaltic flow through the geometry with compliant walls has attained immense interest for the researchers [15]. A lot of literature is available for the study of peristaltic flows in channels, ducts and tubes having compliant walls. Abed Elnaby and Haroun [16] have presented a new model to study the influence of wall properties on peristaltic motion of a viscous fluid. Actually the study of compliant wall is very useful for controlling the Muscle tension. The action of these muscles has been discussed mathematically by a set of equations which relate to compliant wall displacement [17, 18]. Srinivasvas and Kothandapani [19] have achieved the consequences of heat and mass transfer analysis on MHD peristaltic flow across a porous space and considered the wall properties.

The flow having more than one phase of a given fluid occurs is considered as a multiphase flow. Examples of multiphase fluids include gas-liquid transport in evaporators and condensers, gas-liquid-solid flows in chemical reactors, solid-gas flows in pneumatic conveying, etc. It is useful to look at the variegated and ubiquitous challenges of multiphase flow. In fact multiphase flows must occur in processing technology. It is prominently seen in cavitating pumps and turbines to electro photographic processes to papermaking to the pellet form of almost all raw

*Corresponding author: Tel: 3006076036
Fax: 3006076036, e-mail: arshad-riaz@ue.edu.pk

plastics. Multiphase flows are also a prepared aspect of our environment, whether one considers rain, fog, snow, sediment transport, mudslides, debris flows, and many more natural phenomena. Very delicate medical and biological flows are mostly motives, from the blood pumping to semen to the bends to lithotripsy to laser surgery cavitation and so on. There are few studies which deal with the peristaltic multiphase flows [20, 21].

However, the inclusion of MHD and wall properties of the peristaltic multiphase flow of non-Newtonian fluid has not been yet explored. Keeping in mind the highly significant role of compliant walls in peristaltic flows, the authors have a keen interest in presenting the non-Newtonian multiphase fluid in the presence of applied magnetic field in an annulus with complaint walls. The equations governing the problem are reduced to the simple format under the assumptions of the least Reynolds number and large wavelength. The exact solution for obtaining equations under certain boundary conditions has been obtained. The effects of all pertinent parameters are also taken into account graphically.

2. Development of the Problem

In this section, flow through infinite coaxial cylinders is taken into account. The inner gap between both tubes is loaded through irrational, incompressible and non-Newtonian fluid having minor spherical particles. The inward tube is considered as rigid though the external tube is taken as elastic and a sinusoidal wave moving with a steady speed on it. The cylindrical coordinate system (r, z) is chosen such that the radial direction is represented by $\hat{r}$ and $\hat{z}$ is considered along the center point of external and internal tube as sketched in Fig. 1:

The schematic view of the divider surface is along these lines portrayed as

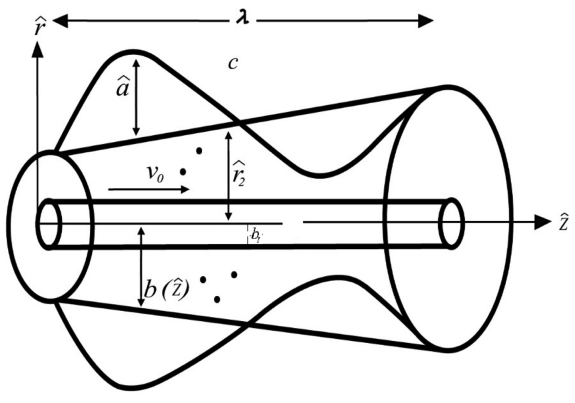

Fig. 1. Diagram of the geometry.

$$\hat{r}_1 = b_1, \quad \hat{r}_2 = b(\hat{z}) + \hat{a}\sin\frac{2\pi}{\lambda}(\hat{z} - c\hat{t}), \tag{1}$$

where

$$b(\hat{z}) = b_0 + \kappa\hat{z}. \tag{2}$$

In above defined equations, the radius of inward tube is represented by, at any axial distance $\hat{z}$ the radius of the external tube from channel is represented by $b(\hat{z})$, which is fixed as $b_0 + k\hat{z}$, where k ($<<1$) is a constant parameter whose magnitudes depend upon the length of the annulus and the exit channel dimension, wave amplitude is represented by, λ is showing the wave length, the speed of the wave spread is represented by c and the time is represented by $\hat{t}$. The governing equation motion for fluid phase and particulate phase are stated as follows:

Fluid phase

Continuity Equation:

$$(1-C)\frac{\partial V_f}{\partial \hat{r}} + (1-C)\frac{\partial U_f}{\partial \hat{z}} + (1-C)\frac{V_f}{\hat{r}} = 0\,, \tag{3}$$

Momentum Equations:

r-component

$$(1-C)\frac{\partial \hat{P}}{\partial \hat{r}} = (1-C)\mu_s\left(\frac{1}{\hat{r}}\frac{\partial}{\partial \hat{r}}\hat{r}S_{rr} + \frac{\partial}{\partial \hat{z}}S_{rz} - \frac{S_{\theta\theta}}{\hat{r}}\right) + CD'(\hat{V}_p - \hat{V}_f), \tag{4}$$

z-component

$$(1-C)\frac{\partial \hat{P}}{\partial \hat{z}} = (1-C)\mu_s\left(\frac{1}{\hat{r}}\frac{\partial}{\partial \hat{r}}\hat{r}S_{rz} + \frac{\partial}{\partial \hat{z}}\hat{r}S_{zz}\right) S + CD'(\hat{U}_p - \hat{U}_f) - \sigma B_0^2\hat{U}_f. \tag{5}$$

Particulate phase

Continuity Equation:

$$C\frac{\partial \hat{V}_p}{\partial \hat{r}} + C\frac{\partial \hat{U}_p}{\partial \hat{z}} + C\frac{\hat{V}_p}{\hat{r}} = 0, \tag{6}$$

Momentum Equations:

r-component

$$C\frac{\partial \hat{P}}{\partial \hat{r}} = CD'(\hat{V}_f - \hat{V}_p), \tag{7}$$

z-component

$$C\frac{\partial \hat{P}}{\partial \hat{z}} = CD'(\hat{U}_f - \hat{U}_p). \tag{8}$$

The stress of Jaffrey fluid [15] is expressed as

$$\boldsymbol{S} = \frac{1}{1+\lambda_1}(\dot{\gamma} + \lambda_2 \ddot{\gamma}), \tag{9}$$

$$\left.\begin{aligned} D' &= \frac{9\mu_0}{2R_0^{\,2}}\hat{\lambda}(\mathrm{C}),\ \mu_s = \frac{\mu_0}{1-\hat{m}C} \\ \hat{\lambda}(\mathrm{C}) &= \frac{4+\sqrt{8C-3C^2}+3c}{(2-3c)^2} \end{aligned}\right\}, \tag{10}$$

$$\hat{m} = 0.70\exp\left[2.49C + \frac{1107}{\hat{T}}\exp(-1.69C)\right]. \tag{11}$$

Here, R_0 representing the radius of every particle, D' is the drag coefficient, C stands for volume fraction density, S represents the stress tensor, μ_s is the viscosity of suspension, the temperature is signified by $\hat{T}$, the viscosity of fluid is μ_0, the ratio between relaxation and retardation time is symbolised by λ_1, delay time is symbolised as λ_2, shear rate is denoted by $\dot{\gamma}$ and dot express the derivative w.r.t. time. Presently, it advantageous to characterize dimensionless quantities as

$$\left.\begin{aligned} &r = \frac{\hat{r}}{b_0},\ z = \frac{\hat{z}}{\lambda},\ U_{f,p} = \frac{\hat{U}_{f,p}}{c},\ V_{f,p} = \frac{\lambda \hat{V}_{f,p}}{b_0 c}, \\ &t = \frac{\hat{t}c}{\lambda},\ p = \frac{b_0^2}{\lambda\mu_0 c}\hat{p},\ \mu = \frac{\mu_s}{\mu_0} \\ &V_0 = \frac{\hat{V}}{c},\ r_1 = \frac{\hat{r}_1}{b_0},\ r_2 = \frac{\hat{r}_2}{b_0},\ \phi = \frac{\hat{a}}{b},\ \delta = \frac{b_0}{\lambda}, \\ &N_1 = \frac{D'b_0^2}{(1-C)\mu_0},\ M = \sqrt{\frac{\sigma}{\mu}}\,b_0 B_0 \end{aligned}\right\}, \tag{12}$$

where wave number is defined by δ, M is the Hartmann number, N_1 represents the drag coefficient parameter and $\phi(< 1)$ is the amplitude ratio. To continue further, consider the assumption of long wave length and creeping flow. Using Eq. (12) in Eq. (3) to Eq. (9), we get:

$$\frac{\partial P}{\partial r} = 0, \tag{13}$$

$$\frac{dP}{dz} = \frac{\mu}{1+\lambda_1}\left[\frac{1}{r}\frac{\partial U_f}{\partial r} + \frac{\partial^2 U_f}{\partial r^2}\right] + CN_1(U_p - U_f) - \frac{M^2(U_f+1)}{(1-C)}, \tag{14}$$

$$\frac{dP}{dz} = (1-C)N_1(U_f - U_p), \tag{15}$$

for complaint walls [15]

$$\frac{dP}{dz} = E_1\frac{\partial^3\eta}{\partial t^2\partial z} + E_2\frac{\partial^2\eta}{\partial t\partial z} + E_3\frac{\partial^5\eta}{\partial z^5} - E_4\frac{\partial^3\eta}{\partial z^3} + E_5\frac{\partial\eta}{\partial z}, \tag{16}$$

where

$$\eta = \phi\sin 2\pi(z-t) \tag{17}$$

From Eq. (13) it is obvious that p is independent of r, hence the relevant BC's are expressed as:

$$\left.\begin{aligned} U_f &= -1 \quad \text{at } \mathrm{r}_1 = \varepsilon, \\ U_f &= -1 \quad \text{at } \mathrm{r}_2 = 1+\phi\,\mathrm{Sin}\,2\pi(z-t) \end{aligned}\right\}. \tag{18}$$

In an above relation, E_i (i = 1, 2, 3, 4, 5) are defined, as $E_1 = \frac{ma^3c}{\lambda^3\mu}$ is wall tension, $E_2 = \frac{Da^3}{\lambda^2\mu}$ is a mass characterization parameter, $E_3 = \frac{Ba^3}{c\lambda^3\mu}$ is damping nature, $E_4 = \frac{Ta^3}{c\lambda^3\mu}$ is wall rigidity and $E_5 = \frac{Ka^3}{c\lambda\mu}$ is wall elastic, are the dimensionless elasticity factors. Here, the mass per unit area is represented by m, the flexural rigidity of the plate is characterized by B, the elastic tension per unit width in the membrane is signified by T, D is the coefficient gives the viscous damping forces and K is the spring stiffness.

Solution of the problem:

Using Eq. (15) and Eq. (18) in Eq. (14), the exact solution with can be written as

$$U_f = \frac{\left(\begin{aligned} &\frac{dp}{dz}(r_1-r_2)(r_1+r_2)(1+\lambda_1)\ln[r] + \\ &\left(-\frac{dp}{dz}(r-r_2)(r+r_2)(1+\lambda_1) - 4(-1+C)\mu\right)\ln[r_1] + \\ &\left(\frac{dp}{dz}(r-r_1)(r+r_1)(1+\lambda_1) + 4(-1+C)\mu\right)\ln[r_2] \end{aligned}\right)}{\left(4(-1+C)\mu\left(\ln[r_1]-\ln[r_2]\right)\right)}, \tag{19}$$

Now using the Eq. (19) in Eq. (15), then we get the exact value of up as follows:

$$U_p = \frac{\frac{4\frac{dp}{dz}}{N_1} + \left(\begin{aligned} &\frac{dp}{dz}(r_1-r_2)(r_1+r_2)\mu\ln[r] + \\ &\left(-\frac{dp}{dz}(r-r_2)(r+r_2)(1+\lambda_1) - 4(-1+C)\mu\right)\ln[r_1] + \\ &\left(\frac{dp}{dz}(r-r_1)(r+r_1)(1+\lambda_1) + 4(-1+C)\mu\right)\ln[r_2] \end{aligned}\right)}{4(-1+C)\left(\mu\left(\ln[r_1]-\ln[r_2]\right)\right)}. \tag{20}$$

The volume flow rate of fluid and dust phase is expressed as

$$Q(z,t) = Q_f(z,t) + Q_p(z,t), \tag{21}$$

where

$$Q_f(z,t) = 2\pi(1-C)\int_{r_1}^{r_2} rU_f\,dr, \tag{22}$$

$$Q_p(z,t) = 2\pi C\int_{r_1}^{r_2} rU_p\,dr. \tag{23}$$

After using Eq. (21) to Eq. (23), the simplified form, volume flow rate is able to express as

$$Q(z,t)=\frac{\left(\pi(r_1-r_2)(r_1+r_2)\left(\begin{array}{l}N_1\dfrac{dp}{dz}(r_1-r_2)(r_1+r_2)(1+\lambda_1)-\\ \left(\begin{array}{l}N_1\dfrac{dp}{dz}(r_1^2+r_2^2)(1+\lambda_1)+\\ 8\left(N_1-CN_1+C\dfrac{dp}{dz}\right)\mu\end{array}\right)\left(\ln[r_1]+\ln[r_2]\right)\end{array}\right)\right)}{\left(8(-1+C)N_1\mu\left(\ln[r_1]-\ln[r_2]\right)\right)}. \tag{24}$$

3. Numerical Results and Discussion

In this session, the solutions are discussed graphically. The graphs for the fluid velocity profile and particle velocity profile are sketched in two dimensions. Velocity profile is plotted for non-Newtonian as a particular case of our study. In order to bring out the addition of dissimilar upper given parameters, computational software Mathematica has been used to visualize the performance of all the parameters through graphs.

3.1. Fluid velocity profile

Figures 2-10 represent the behavior of velocity profiles of fluid beside the different parameters. It can be observed from Fig. 2 that the velocity and volume fraction (C) varies directly. On the other hand, from Fig. 3, it can be noticed that as Hartmann number (M) gets larger, the velocity profile decreases. From Figs. 4-5, it can be easily observed that by increasing weightage of the Jeffery factor parameter λ_1 and the amplitude ratio ϕ, respectively, the velocity field increases and gets absolute maximum value in the Central part of the domain value. Fig. 6 shows that by increasing the values of E_1, the velocity decreases. Figs. 7-10 are plotted to see the effects

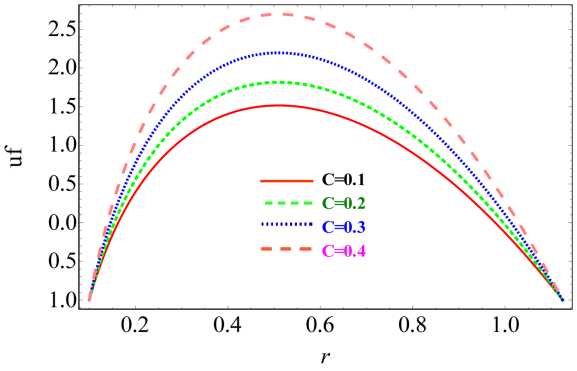

Fig. 2. (Color online) Variation in velocity profile of U_f with r for different values of particle volume fraction C for fixed E_1 = 0.5, E_2 = 0.6, ϕ = 0.5, μ = 1.2, M = 0.1, λ_1 = 37, E_3 = 0.6, E_4 = 0.7, E_5 = 0.9.

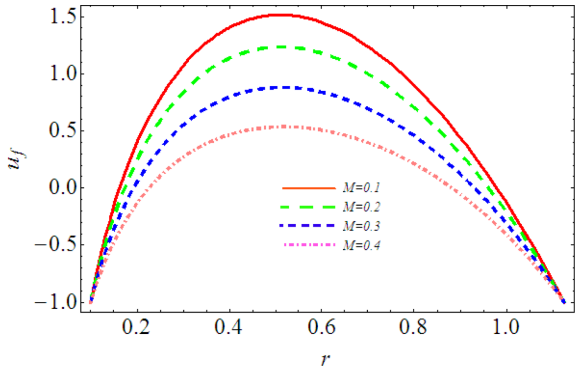

Fig. 3. (Color online) Variation in velocity profile of U_f with r for different values of magnetic field factor M for fixed E_1 = 0.5, ϕ = 0.1, μ = 0.1, C = 0.1, λ_1 = 37, E_2 = 0.6, E_3 = 0.6, E_4 = 0.7, E_5 = 0.9.

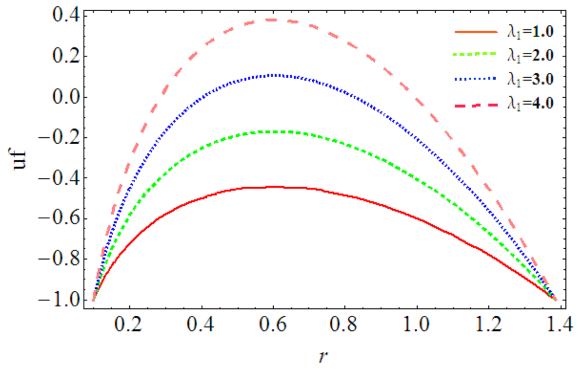

Fig. 4. (Color online) Variation in velocity profile of U_f with r for different values of Jeffery fluid parameter λ_1 for fixed E_1 = 0.5, ϕ = 0.5, μ = 1.2, M = 0.1, C = 0.1, E_2 = 0.6, E_3 = 0.6, E_4 = 0.7, E_5 = 0.9.

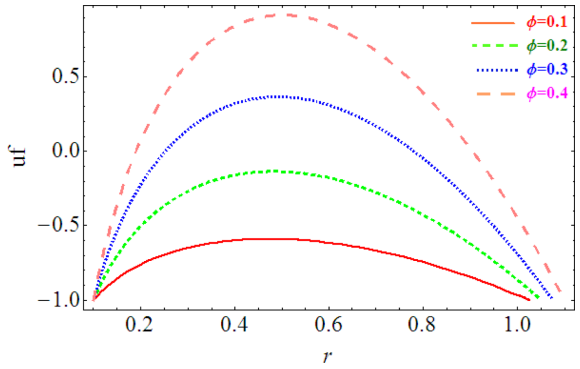

Fig. 5. (Color online) Variation in velocity profile of U_f with r for different values of amplitude ratio ϕ for fixed μ = 1.2, M = 0.1, C = 0.1, λ_1 = 37, E_2 = 0.6, E_3 = 0.6, E_4 = 0.7, E_5 = 0.9.

of different physical parameters namely E_2, E_3, E_4 and E_5 on velocity vector. It can be measured that by increasing the effects of these parameters, the velocity profile increases.

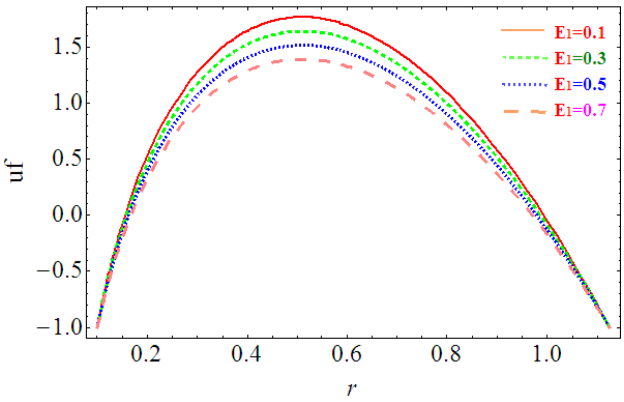

Fig. 6. (Color online) Variation in velocity profile of U_f with r for different values of E_1 for fixed $E_1 = 0.7$, $\phi = 0.5$, $\mu = 1.2$, $M = 0.1$, $C = 0.1$, $\lambda_1 = 3$, $E_2 = 0.6$, $E_3 = 0.6$, $E_4 = 0.7$, $E_5 = 0.9$.

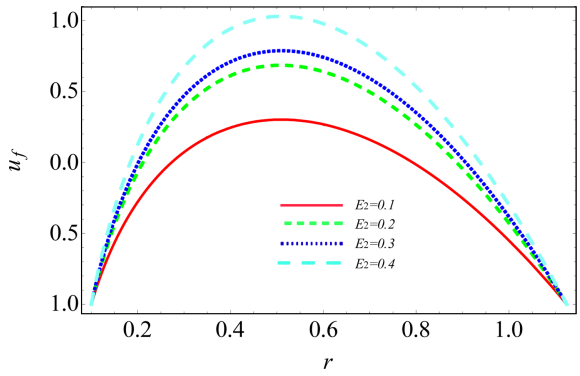

Fig. 7. (Color online) Variation in velocity profile of U_f with r for different values of E_2 for fixed $\phi = 0.5$, $\mu = 1.2$, $M = 0.1$, $C = 0.1$, $\lambda_1 = 37$, $E_1 = 0.5$, $E_3 = 0.6$, $E_4 = 0.7$, $E_5 = 0.9$.

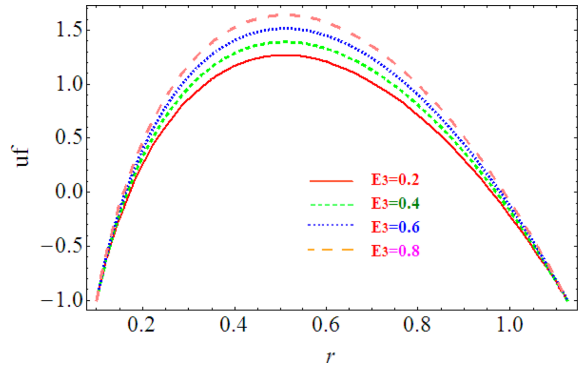

Fig. 8. (Color online) Variation in velocity profile of U_f with r for different values of E_3 for fixed $\phi = 0.5$, $\mu = 1.2$, $M = 0.1$, $C = 0.1$, $\lambda_1 = 37$, $E_1 = 0.5$, $E_2 = 0.6$, $E_4 = 0.7$, $E_5 = 0.9$.

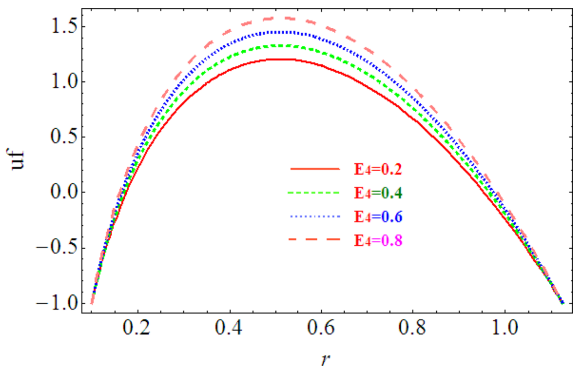

Fig. 9. (Color online) Variation in velocity profile of U_f with r for different values of E_4 for fixed $\phi = 0.5$, $\mu = 1.2$, $M = 0.1$, $C = 0.1$, $\lambda_1 = 37$, $E_1 = 0.5$, $E_2 = 0.6$, $E_3 = 0.6$, $E_5 = 0.9$.

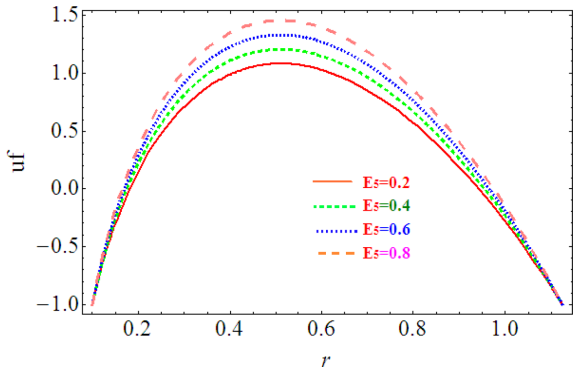

Fig. 10. (Color online) Variation in velocity profile of U_f with r for different values of E_5 for fixed $\phi = 0.5$, $\mu = 1.2$, $M = 0.1$, $C = 0.1$, $\lambda_1 = 37$, $E_1 = 0.5$, $E_2 = 0.6$, $E_3 = 0.6$, $E_5 = 0.7$.

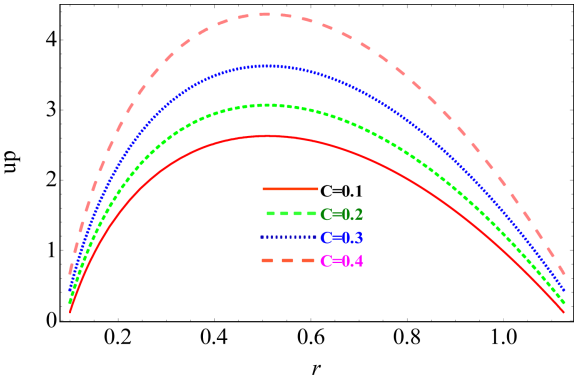

Fig. 11. (Color online) Variation in velocity profile of U_p with r for different values of particle volume fraction C for fixed $\phi = 0.5$, $\mu = 1.2$, $M = 0.1$, $C = 0.1$, $\lambda_1 = 37$, $E_1 = 0.5$, $E_2 = 0.6$, $E_3 = 0.6$, $E_4 = 0.7$, $E_5 = 0.9$.

3.2. Particle velocity profile

Figures 11-19 represent the behavior of velocity profiles of particle against the different parameters. It can be disclosed from Fig. 11 that the velocity field increases by increasing the quantity of volume fraction (C). Fig. 12 tells us some different story; it can be noticed that if Hartmann number (M) makes the velocity of particles come down. It means that presence of magnetic field results in resisting the speed of the particles. From Figs. 13-14, it can be easily observed that by increasing the

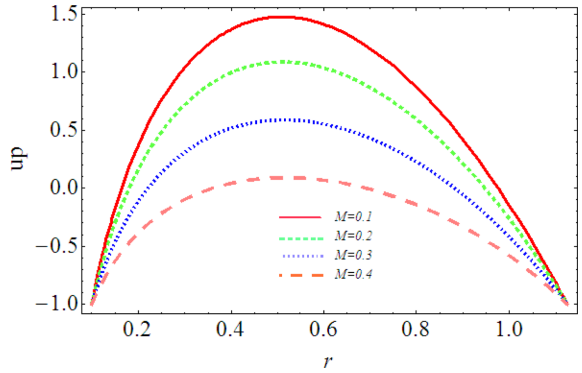

Fig. 12. (Color online) Variation in velocity profile of U_p with r for different values (M) for fixed $\phi = 0.1$, $\mu = 0.1$, $C = 0.1$, $\lambda_1 = 37$, $E_1 = 0.5$, $E_2 = 0.6$, $E_3 = 0.6$, $E_4 = 0.7$, $E_5 = 0.9$.

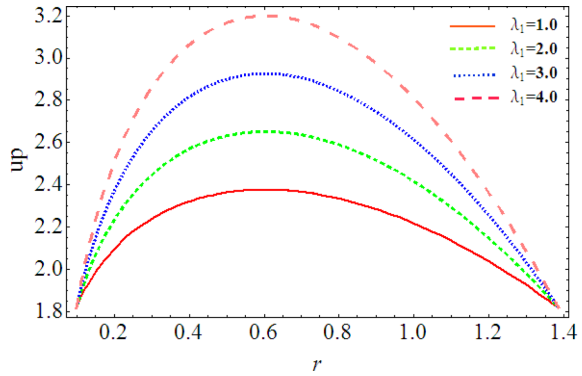

Fig. 13. (Color online) Variation in velocity profile of U_p with r for different values of Jeffery fluid parameter λ_1 for fixed $\phi = 0.5$, $\mu = 1.2$, $M = 0.1$, $C = 0.1$, $E_1 = 0.5$, $E_2 = 0.6$, $E_3 = 0.6$, $E_4 = 0.7$, $E_5 = 0.9$.

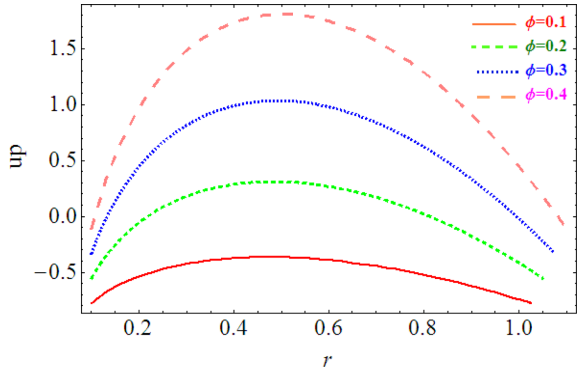

Fig. 14. (Color online) Variation in velocity profile of U_p with r for different values of amplitude ratio ϕ for fixed $\mu = 1.2$, $M = 0.1$, $C = 0.1$, $\lambda_1 = 37$, $E_1 = 0.5$, $E_2 = 0.6$, $E_3 = 0.6$, $E_4 = 0.7$, $E_5 = 0.9$.

Jeffery parameter λ_1 and the amplitude ratio ϕ, respectively, the particle velocity field increases. It reflects the point that when by increasing the relaxation time, the particles move faster. Fig. 15 shows that by increasing the values of, the velocity decreases, which was not in the case for fluid. Figs. 16-19 are plotted to see the effects of different physical parameters namely E_2, E_2, E_3, E_4 and E_5 on velocity vector. It is visible here that by increasing the values of these parameters the velocity profile increases.

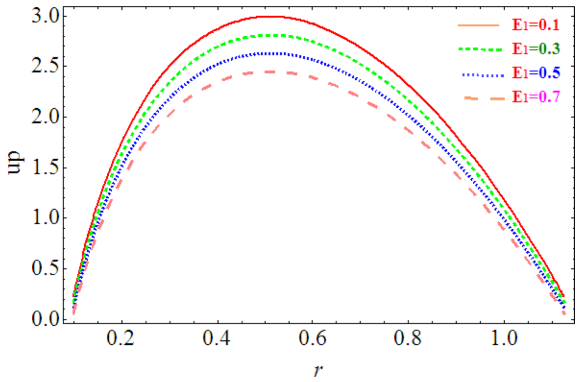

Fig. 15. (Color online) Variation in velocity profile of U_p with r for different values of E_1 for fixed $\phi = 0.5$, $\mu = 1.2$, $M = 0.1$, $C = 0.1$, $\lambda_1 = 37$, $E_2 = 0.6$, $E_3 = 0.6$, $E_4 = 0.7$, $E_5 = 0.9$.

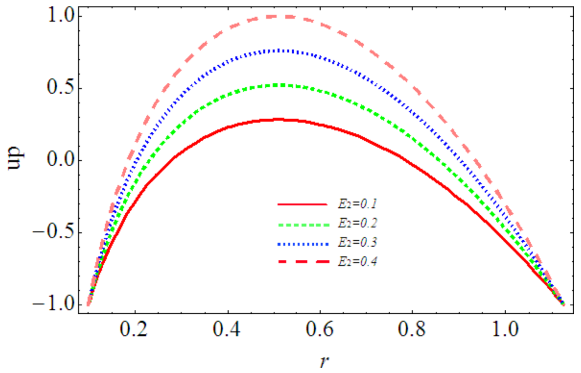

Fig. 16. (Color online) Variation in velocity profile of U_p with r for different values of E_2 for fixed $\phi = 0.5$, $\mu = 1.2$, $M = 0.1$, $C = 0.1$, $\lambda_1 = 37$, $E_1 = 0.5$, $E_3 = 0.6$, $E_4 = 0.7$, $E_5 = 0.9$.

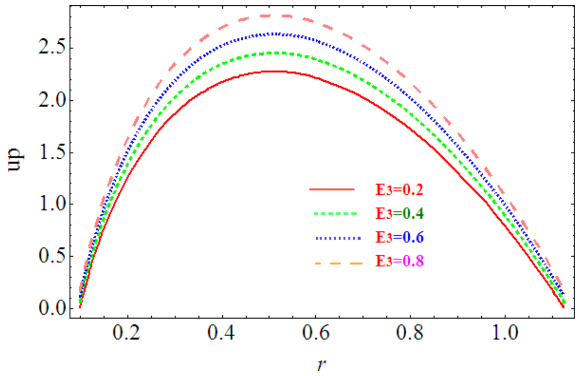

Fig. 17. (Color online) Variation in velocity profile of U_p with r for different values of E_3 for fixed $\phi = 0.5$, $\mu = 1.2$, $M = 0.1$, $C = 0.1$, $\lambda_1 = 37$, $E_1 = 0.5$, $E_2 = 0.6$, $E_4 = 0.7$, $E_5 = 0.9$.

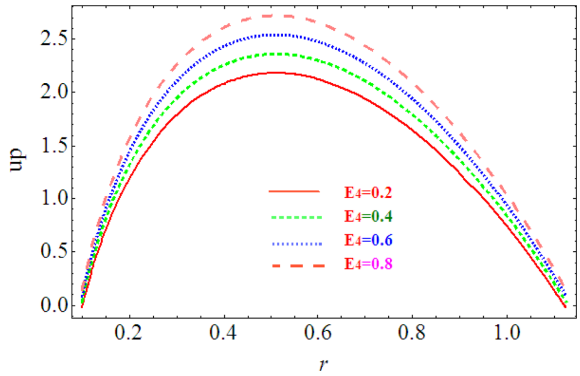

Fig. 18. (Color online) Variation in velocity profile of U_p with r for different values of E_4 for fixed $\phi = 0.5$, $\mu = 1.2$, $M = 0.1$, $C = 0.1$, $\lambda_1 = 37$, $E_1 = 0.5$, $E_2 = 0.6$, $E_3 = 0.6$, $E_5 = 0.9$.

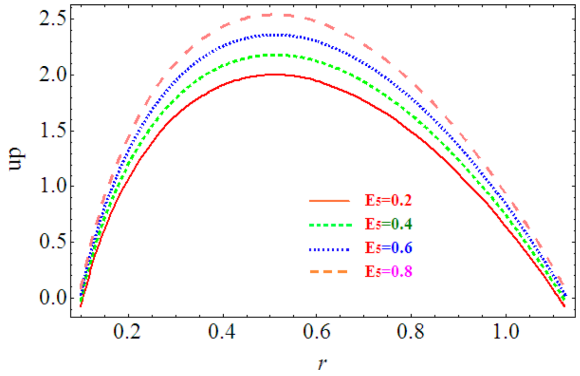

Fig. 19. (Color online) Variation in velocity profile of U_p with r for different values of E_5 for fixed $\phi = 0.5$, $\mu = 1.2$, $M = 0.1$, $C = 0.1$, $\lambda_1 = 37$, $E_1 = 0.5$, $E_2 = 0.6$, $E_3 = 0.6$, $E_4 = 0.7$.

4. Concluding Remarks

This article discusses non-Newtonian multiphase fluid with external MHD in an annulus with complaint walls. The flow is induced by a sinusoidal wave of the external cylinder. The flow is described by law of conservation of mass and momentum. The fluid is assumed to be incompressible. The solution is obtained numerically. The effects of mast parameters are scotched. The major outcomes of our current examination are summarized below:

- From the above mathematical analysis, we have derived that both the fluid and particle velocity profiles diminishes due to the influence of Hartman number while their behavior is opposite for the Jeffery Fluid parameter.
- The fluid and the particle velocities increase with the particle volume fraction and the amplitude ratio, while their behavior is opposite for elasticity parameter.
- For all the remaining elasticity parameters, the fluid and particle velocity profiles vary directly.
- The present analysis can approaches to Newtonian fluid by using $\lambda_1 = 0$, as evidence of novelty and accuracy of the present study.

Nomenclature

$\hat{r}, \hat{z}$	: Cylindrical coordinates
b_1	: Radius of inner tube
$\hat{\alpha}$	: Wave amplitude
c	: Wave speed
λ	: Wavelength
t	: Time
R_0	: Radius of particle
D^t	: Drag Force
C	: Volume fraction density
S	: Stress tensor
μ_s	: Viscosity of suspension
T	: Temperature
μ_0	: Viscosity of fluid
λ_1	: Ratio between relaxation and retardation time
λ_2	: Delay time
$\dot{\gamma}$	: Shear rate
δ	: Wave number
M	: Hartmann number
N_1	: Drag coefficient parameter
ϕ	: Amplitude ratio
E_1	: Wall tension
E_2	: Mass characterization parameter
E_3	: Damping nature
E_4	: Wall rigidity
E_5	: Wall elastic
M	: Mass per unit area
B	: Flexural rigidity of the plate
T	: Elastic tension per unit width
D	: Coefficient of viscous damping forces
K	: Spring stiffness.

References

[1] E. M. Paloka, Math. Mod. Meth. Appl. Sci. **10**, 1425 (2000).
[2] G. Tang, Y. Lu, and Y. Shi, Int. J. Mod. Phy.: Conference Series **34**, 1460385 (2014).
[3] Noreen Sher Akbar, M. Raza, and R. Ellahi, J. Magn. Magn. Mater. **381**, 405 (2015).
[4] K. R. Rajagopal, Int. J. Non-Lin. Mech. **17**, 369 (1982).
[5] R. Ellahi, A. Riaz, S. Abbasbandy, T. Hayat, and K. Vafai, Therm. Sci. **18**, 1247 (2014).
[6] N. S. Akbar, J. Magn. Magn. Mater. **378**, 463 (2015).
[7] E. F. Elshehawey, N. T. Eladabe, E. M. Elghazy, and A. Ebaid, Appl. Math. Comput. **182**, 140 (2006).
[8] S. Srinivas and M. Kothandapani, Int. Commun. Heat Mass **35**, 514 (2008).

[9] S. Nadeem and H. Sadaf, J. Bion. Engng. **14**, 182 (2017).
[10] I. Shahzadi, H. Sadaf, S. Nadeem, and A. Saleem, Comput. Methods Programs Biomed **139**, 137 (2017).
[11] N. S. Akbar and S. Nadeem, Heat Trans. Res. **48**, 283 (2017).
[12] H. Sadaf, S. Nadeem, and Brazilian, J. Soc. Mech. Sci. Engng. **39**, 117 (2017).
[13] S. L. Weinberg, E. C. Eckstein, and A. H. Shapiro, J. Fluid Mech. **49**, 461 (1971).
[14] D. B. Thomas and H. Tin-Kan, J. Fluid Mech. **83**, 249 (1977).
[15] S. Nadeem, A. Riaz, and R. Ellahi, Chem. Ind. Chem. Ingng. Quart. **19**, 399 (2013).
[16] M. A. Abd Elnaby and M. H. Haroun, Commun. Nonlin. Sci. Numer Simul. **13**, 752 (2008).
[17] K. S. Yeo, B. C. Khoo, and W. K. Chong, J. Fluids Struct. **8**, 529 (1994).
[18] N. Takemitsu and Y. Matunobu, Fluid. Dynam. Res. **4**, 1 (1988).
[19] S. Srinivas and M. Kothandapani, Int. Commun. Heat Mass **35**, 514 (2008).
[20] S. Nadeem and I. Shahzadi, Commun. Theor. Phys. **64**, 547 (2015).
[21] J. J. Lozano, M. Sen, and E. Corona, Acta. Mechanica. **219**, 91 (2011).